Annu. Rev. Mater. Sci. 1997. 27:147–73

BINDER REMOVAL FROM CERAMICS

Jennifer A. Lewis
Materials Science and Engineering Department and Beckman Institute, University of Illinois, Urbana, Illinois 61801; e-mail: jalewis@uiuc.edu

KEY WORDS: binder thermolysis, polymer degradation, mass transport, porous materials, platicizers

ABSTRACT

The physico-chemical processes that occur during binder thermolysis of porous ceramic bodies are reviewed. The discussion initially focuses on intrinsic and extrinsic mechanisms of polymer degradation, with emphasis on the formation of volatile degradation products and involatile carbonaceous residue. The transport of volatile species (e.g. residual solvents, plasticizers, etc) and degradation products through both empty and binder-filled pores is then considered. The particular case of debinding highly loaded ceramic bodies is addressed in detail. Recent developments in modeling the onset of defect formation and the effects of capillary redistribution of thermoplastic binders on removal kinetics are outlined. On the basis of this fundamental knowledge, the criteria for optimizing binder removal processes is established.

INTRODUCTION

Ceramic powders are inherently difficult to handle and shape into desired components because of their discreet nature and lack of cohesiveness and plasticity. Organic processing aids, such as polymers (or binders), plasticizers, dispersants, and solvents, are therefore often required to enhance their forming capabilities. The term binder system is used to collectively describe those additives that remain in the as-formed ceramic body after drying. Such additives are transient aids that must be removed completely prior to component densification at elevated temperatures. This process is known as binder removal.

Several strategies have been proposed to debinderize ceramic components including (*a*) thermal debinding, (*b*) wicking, (*c*) solvent extraction, and (*d*) supercritical fluid extraction. Of these, thermal debinding (or binder thermolysis) remains the most widely utilized process in the manufacture of traditional

0084-6600/97/0801-0147$08.00

and advanced ceramic components and is the subject of this review. Many complex chemical and physical processes occur, often simultaneously, during binder thermolysis: decomposition of organic species; chemical interactions between these species and the surfaces of ceramic powders; mass transport of reactants, volatile species, and degradation products through binder-filled and empty pores; and changes in the distribution of condensed binder within the pore structure of the ceramic body. In practice, binder removal can be difficult to control, thus leading to a variety of defects that reduce the yield of ceramic manufacturing processes. For instance, carbon retention, cracking, blistering, warping, anisotropic shrinkage, and delamination of fired bodies can all result from inadequate binder removal. Throughput is another important issue; for example, thermal debinding of highly loaded ceramic green bodies (e.g. injection-molded parts) often requires several days to complete. To fully optimize binder formulations and removal conditions for successful debinding of ceramic components, a mechanistic understanding of the complex physicochemical processes that occur during binder thermolysis is required. Within the past decade, research activities have been initiated with the aim of developing this fundamental knowledge base. In this review, we begin with a brief discussion of binder systems, highlighting their historical development, primary functions, and important properties. Next, we detail the chemical and physical processes that occur during binder thermolysis, as currently understood. Finally, we point out existing deficiencies in this emerging knowledge base and offer suggestions for future research activities.

BINDER SYSTEMS, FUNCTIONS, AND PROPERTIES

Much of the early work on binder systems focused on developing suitable formulations for a given processing sequence (1–9). Whittemore (1) and Wild (2) provide excellent summaries of the historical use of organic (and inorganic) binder systems in ceramics processing in the early- to mid-1900s. More recent reviews are provided by Pincus & Shipley (5) and Mizuno et al (10), with the latter providing an overview of Japanese patents on organic binder systems. Although such additives were recognized as transient aids from the beginning, little attention was given to binder removal processes in these early communications. Levine (6) appears to be the first researcher to quantitatively study "binder burnout," albeit a secondary consideration in his work, using thermogravimetric analysis (TGA). However, Hoffman (7) must be credited with first detailing the critical effects that organic binders can have on a variety of ceramic fabrication processes. Despite this recognition in the early 1970s, most fundamental studies of the effects of organic additives on microstructural evolution of ceramic bodies have been carried out only within the last decade.

Binder systems provide an array of useful functions in ceramics processing, as listed in Table 1, for several types of organic additives (5). Ceramic forming methods rely on organic additions to various extents; among the most common are dry pressing, isostatic pressing, tape casting, slip casting, extrusion, and injection molding. The selection of a given forming method, determined by considering factors such as part geometry and complexity, the dimensional tolerances required, the quantity to be produced, and cost, has a strong influence on the binder system formulation and loading. Typically, such systems comprise between approximately 5 and 40 vol% of a given ceramic green body, depending on the chosen forming method.

Polymeric and plasticizing species are the primary constituents of most binder systems. Polymeric additives enhance the strength of green bodies by binding the ceramic particles together. Their binding action results from either (*a*) the physical wetting of the particulate surfaces or (*b*) the chemical adsorption of organic functional groups onto the particulate surfaces (11). These additives usually consist of a backbone of covalently bonded carbon-carbon (C–C) linkages, with side groups attached at frequent intervals along the length of the molecule. Polymers are often classified into one of two groups: thermoplastic or thermosetting resins. Thermoplastics are linear polymers with secondary (weak) bonding between side groups, which become molten or fluid upon heating. In contrast, thermosets are covalently bonded, three-dimensional networks that do not flow when heated. Ultimately, all polymers decompose to form volatile degradation products when heated above their respective decomposition temperatures. Thermoplastics such as carbohydrate-derived vinyl- or acrylic-based polymers are the most widely used ceramic processing additives (12) and are

Table 1 Functions of organic additives used in ceramics processing[a]

Additive	Function
Common	
Polymer	Green strength
Plasticizer	Rheological aid; improves flexibility of binder films; allows plastic deformation granules
Dispersant	Steric dispersion
Less Common	
Lubricant	Mold release; interparticle sliding
Wetting agent	Lowers surface tension of liquid
Water retention agent	Prevents squeezing out of water during pressing
Antistatic agent	Charge control
Antifoaming agent	Prevents foam or strengthens desired foams
Chelating agent	Inactivating undesirable ions
Fungicides/bactericides	Stabilizing against degradation with aging

[a]From Reference 5.

the focus of this review, although some use of thermosets (3) has been reported. Characteristic features of polymeric binders include the dimensionality of the covalently bonded network, the type of functional groups, and their molecular chain length, weight, and distribution. These features determine properties such as viscosity of polymer solutions and melts and the cohesion and bonding strength of polymer-derived films, as well as their interactions with ceramic surfaces.

Plasticizers are lower molecular weight species relative to their polymeric counterparts and must be chemically compatible with solvent(s) and polymeric aids. Factors that affect compatibility include the polarity, size, and shape of the plasticizing molecules. In most cases, plasticizers have a high degree of solvent power for the polymer. However, their volatility is much lower than that of most organic solvents, hence plasticizers remain in green bodies processed under ambient conditions. Plasticizers adsorb on the polymer and reduce the secondary valence forces between linear polymer chains; this results in a softened polymer with added flexibility (13) and a lowered glass transition temperature (T_g) (14, 15). Although they soften polymers, plasticizers also tend to reduce the green strength of the ceramic body (12).

POLYMER DEGRADATION

Polymer degradation is achieved by thermal and/or oxidative mechanisms depending on the atmosphere present during binder thermolysis. As heat is applied, polymers degrade to produce volatile species that must diffuse to the green body surface where they can be eliminated. Several variables can affect polymer degradation processes including (*a*) polymer chemistry and structure, (*b*) polymer loading, (*c*) chemical interactions at polymer-ceramic interfaces, (*d*) heat/mass transport, (*e*) component geometry, (*f*) firing atmosphere, and (*g*) heating cycle. In this section, we begin with a discussion of intrinsic polymer degradation mechanisms in the absence and presence of oxidative effects. We then discuss the influence of extrinsic ceramic surface interactions on polymer degradation. One focal point is the identification of the type of volatile species generated and the temperature range over which decomposition occurs for common organic binders, and a second focal point is the identification of side reactions (e.g. cyclization, cross-linking, or surface interactions) that lead to the deleterious formation of residual carbon during binder thermolysis. To simplify the discussion, mass/heat transfer considerations are neglected.

Intrinsic Degradation Mechanisms

There is an extensive body of literature devoted to polymer degradation studies, which has provided a point of departure for many recent investigations of binder

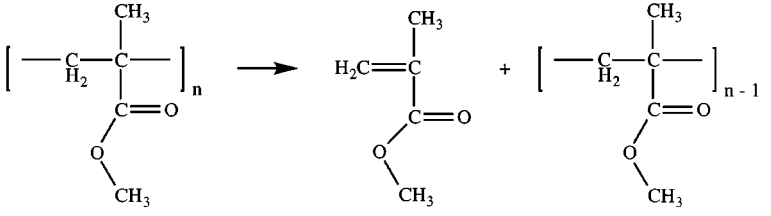

Figure 1 Thermal degradation of poly(methyl methacrylate) (PMMA) by depolymerization.

decomposition in the presence of ceramic materials. One noteworthy deficiency of most pure polymer decomposition studies, however, is the lack of quantitative information regarding involatile carbon residue yields, as they are primarily concerned with understanding initial polymer degradation mechanisms and the compositions of volatile product species (16). Here, we begin with a general overview of the intrinsic polymer degradation mechanisms. This is illustrated through selected examples for polymers commonly used in ceramic processing. Attention is also given to the mechanisms of carbon residue formation and involatile yields of such polymeric additives. For a detailed analysis of reaction kinetics, interested readers are referred to the review by Jellinek (17).

Polymers undergo a variety of intrinsic degradation processes during thermolysis, including depolymerization, random scission, and side group elimination, that produce volatile degradation products, and side reactions such as cyclization and cross-linking that lead to the formation of residual carbon (17). Depolymerization and random scission represent two limiting cases whose reaction kinetics have been treated (17); between these two ends of the degradation spectrum lie all possible transitions (whose kinetic treatment can become quite complicated).

Depolymerization, referred to as unzipping, produces volatile molecular fragments that are practically all monomeric. It can be initiated thermally or by radiation—if chain ends preferentially adsorb this radiation (17). Poly(propylene carbonate) (PPC), poly(butyl methacrylate) (PBMA), and poly(methyl methacrylate) (PMMA) each decompose by unzipping following a sequence similar to that shown in Figure 1 for PMMA. Little has been published on the thermal degradation of PPC (18); however, the intrinsic degradation of methacrylate polymers has been extensively studied (16, 18–24). PMMA has been shown to degrade cleanly (with negligible carbon residue) over a narrow temperature range to yield from 95 to 100% monomer in vacuum or inert atmospheres (16, 18, 24).

Random scission, which can be initiated thermally or by oxidative degradation (17), produces a wide spectrum of molecular fragments that contain

minimal monomer. Poly(ethylene oxide) (PEO) or poly(ethylene glycol) (PEG), as it is usually referred to for lower molecular weight chains, initially degrades by random scission. It has been shown that about 90% of this polymer degrades into waxy substances with an average molecular weight of 675 g/mol which are volatile at elevated temperatures (350°C) (25). Substantial carbon residue formation has been observed during thermal degradation of PEO, which likely arises due to cross-linking reactions between initially scissioned chains (16).

Side group elimination produces an array of low molecular weight species as a result of scission of attached pendant groups along the polymer chain backbone. It can also be initiated thermally or by oxidative degradation (17). Poly(vinyl butyral) (PVB), poly(vinyl alcohol) (PVA), and poly(vinyl acetate) (PVAc) initially degrade by side group elimination following a sequence similar to that shown in Figure 2 for PVB. Initial PVB degradation involves the loss of water, butanal, and acetic acid, leaving long organic chains containing appreciable unsaturation and conjugation. Such chains subsequently degrade by scission, with concurrent cyclization and cross-linking reactions to yield significant amounts of carbon residue (16, 26–29). Polymers such as PVB and PEO, which undergo multi-step degradation processes, typically form volatile species over a relatively broad temperature range.

Side reactions such as cyclization and cross-linking are considered deleterious because they lead to the formation of involatile carbonaceous residue. Residual carbon produced from the thermal degradation of polymeric species will have one of two forms, as illustrated in Figure 3 (16). Pseudographitic carbon, which is composed of multiple polycyclic groups, similar to graphite, results from cyclization reactions. Only a relatively small number of aromatic groups are needed to form a compound that is sufficiently involatile at elevated temperatures (e.g. 1000°C). In contrast, a highly branched, non-aromatic carbon residue forms as a result of cross-linking reactions. It is also conceivable that carbon residue containing a mixture of these two forms could be produced.

The elimination of involatile carbonaceous residues in the final stage of binder removal requires the presence of an oxidative atmosphere. However, such conditions are not always feasible for a given processing sequence. For example, the fabrication of multilayer, co-fired ceramic packages have among the most stringent environmental requirements to avoid unwanted oxidation of metallized conduction lines. In such cases, it is often easier to select additives that volatilize efficiently in inert atmospheres, as opposed to designing an elaborate binder removal process to minimize carbon retention. Higgins (16) has carried out the most extensive study of carbon residue formation during intrinsic thermal decomposition of organic additives widely used in ceramics processing. In his work, specimens were heated to 1000°C at 5°C/min in gettered argon [$<10^{-7}$ ppm O_2(g)] and then cooled to ambient conditions in the same gaseous

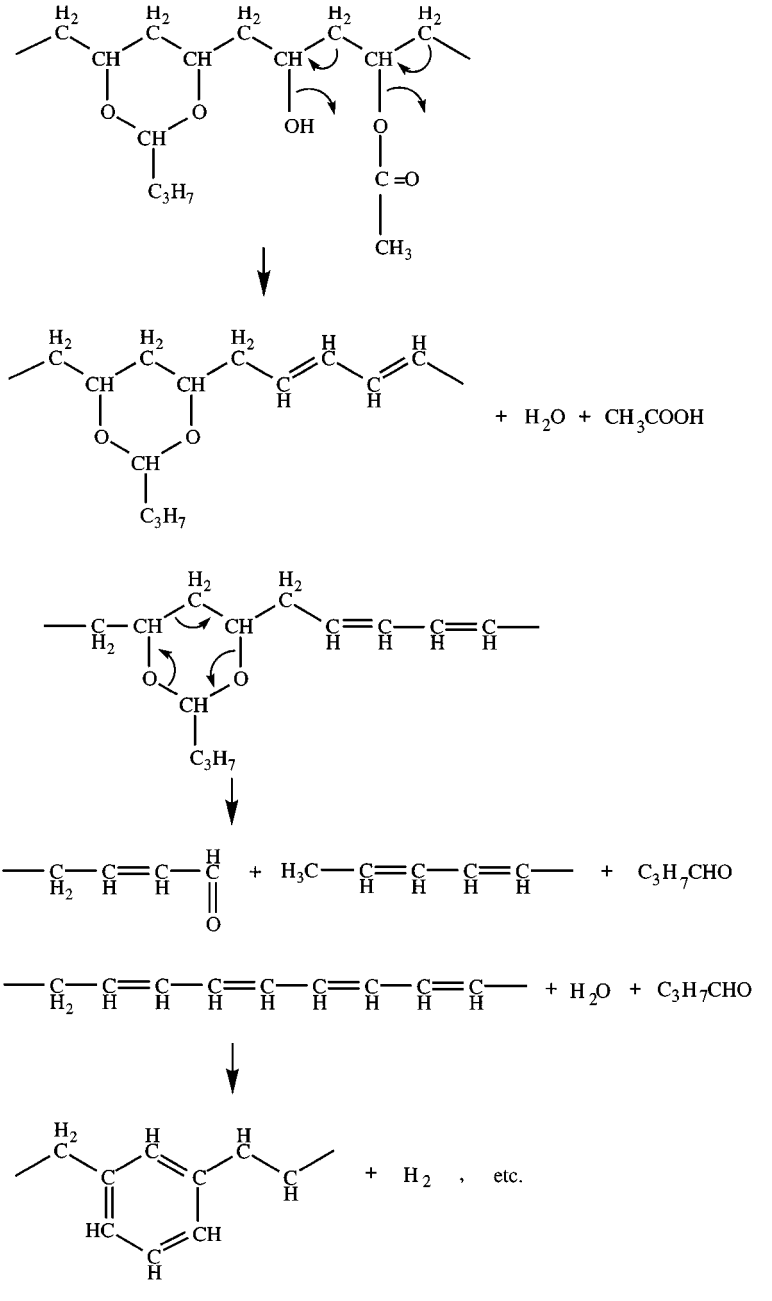

Figure 2 Thermal degradation mechanisms of poly(vinyl butyral) (PVB).

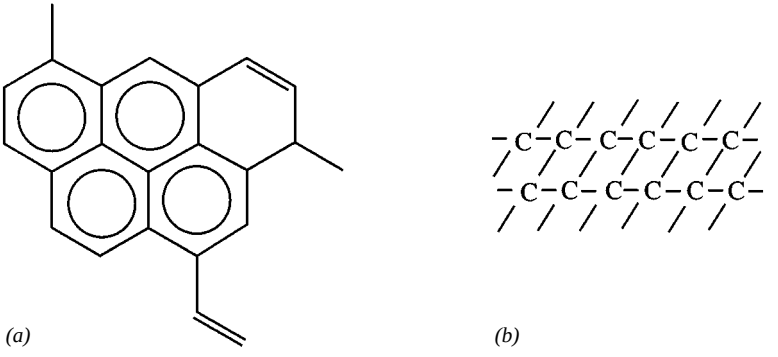

Figure 3 Schematic illustration of the chemical structure of carbonaceous residue: (*a*) pseudographitic and (*b*) cross-linked.

environment. The intrinsic yield of carbonaceous residue for additives studied is reported in Table 2. There are several noteworthy observations: First, polymers that initially decompose by side group elimination and those containing polar functionalities that initially degrade by random scission processes produce appreciable amounts of involatile carbonaceous residue. Cellulosic polymers, which inherently contain cyclic backbone structures, were among the "dirtiest" additives tested with intrinsic yields exceeding 6.0 ± 0.3 wt%. Second, short-chain oligomeric additives (e.g. Menhaden fish oil) can themselves produce a significant quantity of carbon residue. Finally, polymers that decompose via depolymerization and hydrocarbon polymers [e.g. poly(ethylene)] that degrade by random scission into volatile alkanes and alkenes appear to be among the "cleanest" additives studied (16).

Oxidative atmospheres can either accelerate or inhibit polymer degradation reactions; their effect depends on the specific polymer as well as the temperature range (or stage of decomposition). For example, oxygen inhibits decomposition of PMMA initially (200–300°C), while at higher temperatures it accelerates decomposition by enhancing random scission events (22). Often binder removal is carried out in an oxygen-containing environment, so attention must be given to both thermal and oxidative degradation processes. The role of oxygen can be complex, as the above example illustrates; however, as discussed previously, it is generally beneficial in eliminating unwanted carbonaceous residue.

Ceramic Surface Interactions

Polymer degradation occurs in the presence of ceramic surfaces during binder removal. Such surfaces contain acidic and/or basic sites that can catalyze cracking and isomerization reactions as well as promote cross-linking during thermolysis. It is well known that oxide surfaces contribute to carbon formation

Table 2 Carbon residue yields for different organic additives heat treated in an inert atmosphere to 1000°C[a]

Organic compound	Carbon residue yield (wt%)[b]
Polyethylene	<0.1
Polyisobutylene	<0.1
Polypropylene carbonate	<0.1
Polymethyl methacrylate	
low mol. wt.	0.2 ± 0.1
medium mol. wt.	0.2 ± 0.1
high mol. wt.	0.2 ± 0.1
Polybutyl methacrylate	0.2 ± 0.1
Polyethylene oxide	
3,400 g/mol	0.3 ± 0.1
20,000 g/mol	2.5 ± 0.1
100,000 g/mol	3.1 ± 0.2
600,000 g/mol	4.5 ± 0.2
Polyvinyl butyral	
Butvar B-76	1.8 ± 0.1
Butvar B-98	1.3 ± 0.1
Menhaden fish oil	3.5 ± 0.2
Cellulose	10.5 ± 0.5
Ethyl cellulose	6.0 ± 0.3

[a]From Reference 16.
[b]Based on initial sample weight.

processes (30–33). The carbon that forms is named by examining its source; a hydrocarbon source forms coke, whereas a polymeric source forms polymeric (or residual) carbon. The role oxide surfaces play in coke formation is important in several fields, e.g. oxide activators (34) are used in the cross-linking (non-sulfur vulcanization) of natural rubber, and alumina-silica catalysts (35) are used in the cracking of petroleum feedstocks. Here, we review the limited work carried out to date that probes the effects of ceramic surface interactions on polymer degradation processes and carbon retention during non-oxidative binder thermolysis.

The most comprehensive studies have focused on PMMA-oxide surface interactions (16, 24, 36–38). PMMA is widely utilized in such studies because its thermal degradation chemistry is both well known and relatively simple. As discussed above, neat PMMA thermally decomposes in inert environments with negligible production of involatile carbonaceous residue. However, Higgins (16) has shown that PMMA/oxide compacts heated to 1000°C at 5°C/min in gettered argon (10^{-7} ppm oxygen) can retain appreciable amounts of residual carbon, as shown in Figure 4, depending on the oxide surface chemistry. In the presence of amphoteric alumina (α-Al_2O_3) surfaces, residual carbon contents

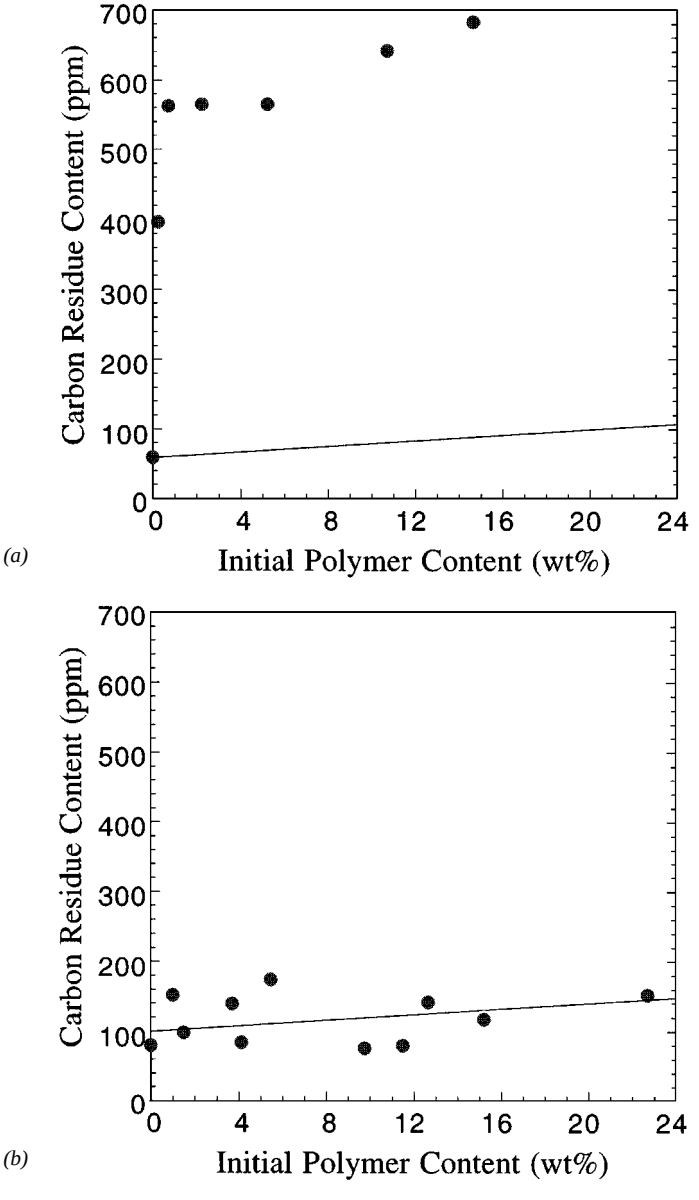

Figure 4 Plots of carbon-residue contents of (*a*) PMMA/aluminum oxide (α-Al_2O_3) and (*b*) PMMA/silicon oxide (SiO_2) composite films with varying PMMA loading (expressed as wt% of initial film weight) heat-treated in gettered argon to 1000°C. (*Solid line* corresponds to predicted carbon residue contents calculated by summing the inherent carbon contamination level present in the starting ceramic powders and the involatile carbon residue yields predicted solely on the basis of intrinsic degradation processes.) (from Reference 16, 36)

exceeding 500 ppm were observed for initial PMMA loadings in excess of 0.5 wt%. The consistent carbon residue yields observed in compacts with widely varying initial PMMA loadings suggest that the α-Al_2O_3 surface plays a stoichiometric and irreversible role in residue production (36). In contrast, acidic silica (SiO_2) surfaces appear to have a negligible effect on residual carbon contents, suggesting that such surfaces do not interact significantly with PMMA or its degradation products (36, 37).

Sun et al (24) were first to report on the chemical interactions between PMMA and α-Al_2O_3 surfaces during thermal degradation. Building on these observations, Higgins et al (36) carried out a detailed study of such interactions using Fourier transform infrared (FTIR) spectroscopy and evolved gas analysis utilizing mass spectral detection. They showed rather convincingly that organic groups bind to surface hydroxyl groups present on α-Al_2O_3 particles by a sponification reaction (39) between either the ester groups of PMMA or thermally evolved PMMA fragments (including monomer) via the following reaction:

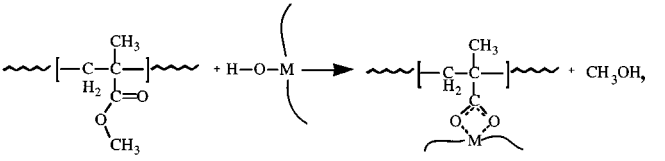

1.

where $M = \text{Al}$, in this case. This reaction anchors organic residue to the inorganic surface to temperatures well above the unzipping temperature of the pure polymer and leads to the retention of organic fragments in compacts where neat PMMA has completely volatilized (see Figure 4) (36). Hirakata et al (38) has probed the effects of complex, multi-cation oxide surfaces (i.e. lead titanate) with Pb/Ti molar ratios of 0.92 to 1.08 on PMMA degradation, and found that carbon residue contents varied from 0.2 to 1.2 mg/m^2 for samples heated to 600°C in nitrogen, respectively. They also found that the ester groups of PMMA or thermally evolved monomer reacted with surface hydroxyls on the lead titanate powder (where M = Pb, Ti in Equation 1). The influence of Pb/Ti molar ratio on carbon retention was correlated to changes in the reactivity of such sites. Although Ti-rich powders contained a higher concentration of surface hydroxyls, those sites were shown to be more acidic (less reactive) in nature, leading to the observed trend in carbon retention (38).

Significant activity (27–29, 40, 41) has also been directed toward understanding the effects of ceramic surfaces on the thermal degradation of PVB due to its wide utilization in fabricating ceramic thick films for electronic packaging applications. However, relative to the case of PMMA, the mechanistic understanding is somewhat limited due to the increased complexity of pure PVB degradation and volatile product composition. As discussed above, neat PVB

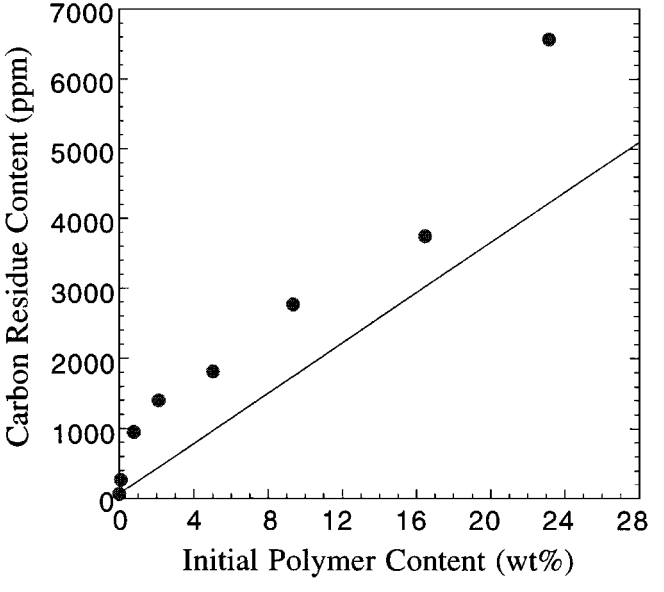

(a)

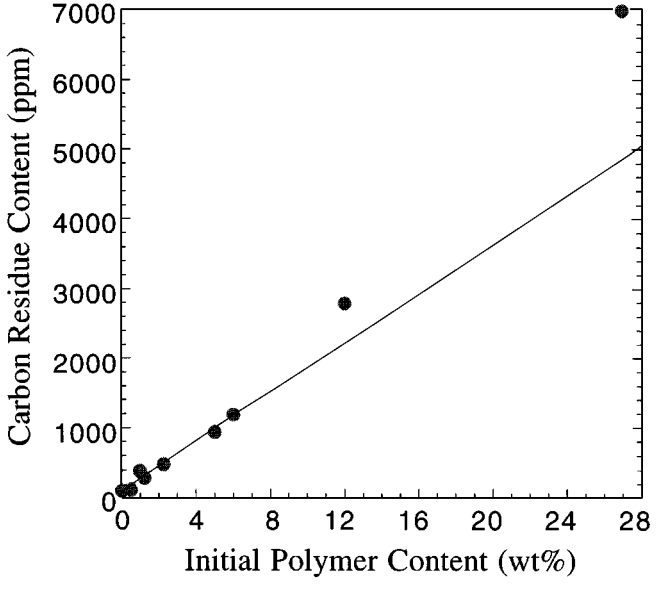

(b)

Figure 5 Plots of carbon-residue contents of (*a*) PVB/aluminum oxide (α-Al_2O_3) and (*b*) PVB/silicon oxide (SiO_2) composite films with varying PVB loading (expressed as wt% of initial film weight) heat-treated in gettered argon to 1000°C (*Solid line* corresponds to predicted carbon residue contents calculated by summing the inherent carbon contamination level present in the starting ceramic powders and the involatile carbon residue yields predicted solely on the basis of intrinsic degradation processes.) (from Reference 16.)

thermally decomposes in inert environments with appreciable production of involatile carbonaceous residue (>1 wt%). Nair & White (41) have shown that oxides such as α-Al_2O_3, SiO_2, and mullite catalyze the production of butanal, which is formed initially during degradation as a result of side group elimination. Higgins (16) has studied carbon retention of PVB/oxide compacts heated to 1000°C at 5°C/min in gettered argon (10^{-7} ppm oxygen). The residual carbon contents of such samples, shown in Figure 5, were found to be much higher than those observed in related work on PMMA/ceramic surface interactions (see Figure 4). Such differences can be traced primarily to significant differences in their intrinsic yield of involatile carbonaceous residue. However, the respective influences of amphoteric α-Al_2O_3 and acidic SiO_2 surfaces on carbon retention followed the same trends for PVB degradation as those observed for PMMA degradation.

Extrinsic effects stemming from ceramic surface interactions can greatly impact polymer degradation processes. There is clearly a need to extend the limited studies discussed above to explore the interactions between a broader range of common polymeric additives and various single- and multi-cation ceramic oxide and nonoxide surfaces, with emphasis on both catalytic effects leading to accelerated degradation and side reactions leading to carbon residue formation.

MASS TRANSPORT

Several mass transport processes often occur simultaneously during binder removal. As heat is applied, volatile constituents diffuse to the surface of the green body (or penetrating binder-vapor interface) where they evaporate. Such species must be transported through both binder-filled pore channels and through regions of the green body that are devoid of binder (i.e. empty pores). In a mathematical sense, the distribution of the binder and the outer surfaces of the green body define the boundary conditions for mass transport. The binder distribution within the green body determines the path length over which volatile materials must diffuse to reach the binder-vapor interface, whereas the pore structure of the green body influences the resistance to mass transfer. Schematic representations of the binder-vapor interface evolution during binder thermolysis of a highly loaded green body are shown in Figure 6. As volatiles are removed from the green body, empty pore space is created. The binder-vapor interface, shown to penetrate toward the interior of the green body in either a planar or nonplanar front, represents a boundary between diffusion of volatiles in the organic phase (e.g. molten polymer) and in the gaseous phase (i.e. empty pores). Because of differences in volatile diffusivities between these two phases, the processes by which binders distribute within the green body during thermolysis are intimately coupled to their removal kinetics.

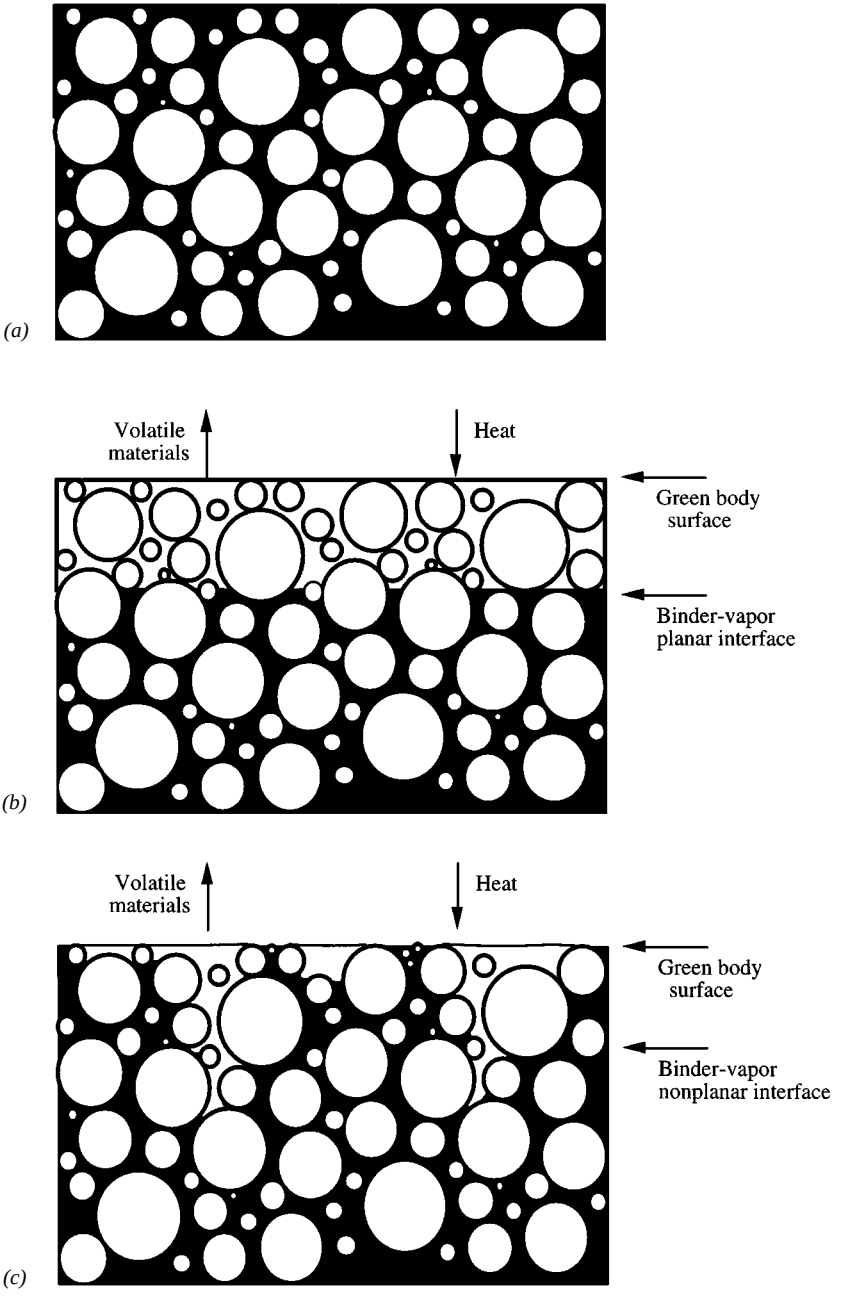

Figure 6 Schematic illustrations of binder-vapor interface development in closed-pore compacts during binder thermolysis: (*a*) initial binder-vapor interface, (*b*) planar interface, and (*c*) nonplanar interface.

Forming methods that employ low levels of binder (<10 vol%), e.g. pressing operations, slip casting, or centrifugal casting, produce green bodies that have sufficient open porosity to allow volatile materials to escape from the interior to the compact surface. These green bodies are referred to as open-pore compacts. The connected porosity serves as a fast diffusion path for volatile transport, making such compacts relatively easy to debind (unless their outer dimensions exceed several centimeters). In contrast, forming methods like tape casting and injection molding produce green bodies that contain much higher binder loadings (15–50 vol%). Such bodies are referred to as closed-pore compacts because their void space is nearly or completely filled with binder. In this case, there is an initial absence of connected pore space (i.e. fast transport path), which is the primary reason why successful debinding of these compacts is so difficult.

In this section, we begin with a discussion of volatile transport processes in both open and binder-filled pores. We then discuss binder distribution processes during thermolysis, with an emphasis on capillary-driven transport. A scaling model is presented to predict the length scale over which molten binder can be redistributed by capillary forces within the porous network of the green body. One focal point of this section is to identify possible rate-limiting transport processes; a second focal point is the identification of processes that lead to defect formation during binder thermolysis. To simplify the discussion, heat transfer considerations are neglected. Such effects would be rate-determining only when volatilization rates are quite high, i.e. when defect formation is likely.

Volatile Transport Processes

During binder thermolysis, both volatile species and degradation products must be removed from the green body. Volatile species constituents such as residual solvent, plasticizers, and other low molecular weight components in the binder system are present within the green body at some initial concentration and have an appreciable vapor pressure relative to the polymeric constituents. As these species diffuse to the surface of the green body and evaporate, their concentration decreases. In contrast, volatile degradation products (e.g. monomers, dimers, etc) have an initial concentration equal to zero, but their concentration grows as degradation reactions proceed and then diminishes as they diffuse to the surface of the green body. Polymeric constituents degrade rather than vaporize as this process is energetically more favorable (17). Degradation products can be considered to be volatile when their chain lengths are less than or equal to the ratio of energy required to break a main chain bond to the heat of vaporization of the monomer. In the case of polystyrene, this ratio amounts to roughly 7 (i.e. 62 kcal/mol divided by 9 kcal/mol), hence products of up to heptamers in length can vaporize (17).

Gas-phase transport plays an important role in binder thermolysis. In fact, it is likely the dominant transport process during debinding of open-pore compacts. In contrast, it contributes little initially during debinding of closed-pore compacts, but becomes increasingly important as removal progresses. In both cases, the removal of carbonaceous residue during the later stage of binder thermolysis relies on both in-diffusion of oxidative species and out-diffusion of gaseous products.

Transport of gaseous species through empty pores occurs by either Knudsen, slip, or viscous (Poiseuille) flow (42–44). Knudsen flow (45) occurs when the average pore radius (r) is much smaller than the mean free path (λ_g), $r/\lambda_g < 0.1$. Slip flow occurs when gas transport is intermediate between viscous flow and Knudsen flow, i.e. r/λ_g is in the range of 0.1 to 10 and, finally, viscous flow occurs when $r/\lambda_g > 10$. Tsai (43) has shown that gas flow in the empty pores of many densely packed ceramic green bodies should be in the transient (slip flow) range.

German (46), Song et al (44), and Tsai (43) have developed models that focus on gas phase transport processes during binder thermolysis of closed-pore compacts. In each case, pore development was modeled as a receding planar front, i.e. capillary redistribution of binder was ignored. The German (46) model considered both Knudsen diffusion and viscous flow, but neglected to account for transport of volatile materials in binder-filled pores. This approach was applied only to predict dewatering of porous beds. The numerical model of Song et al (44) accounted for each of the different gas-flow regimes, as well as transport of degradation products in binder-filled pores. The following expression, developed by Wakao et al (47), was used in their work to estimate K, the transport coefficient for a single gas through a capillary of radius r:

$$K = \frac{1}{RT}\left[\frac{\frac{2r}{3}\sqrt{\frac{8RT}{\pi M_w}}}{1+2r/\lambda} + \frac{1}{1+\lambda/(2r)}\left(\frac{\pi r}{6}\sqrt{\frac{8RT}{\pi M_w}} + \frac{r^2 P}{8\eta}\right)\right], \qquad 2.$$

where R is the gas constant, T is temperature, M_w is molecular weight of the gaseous species, P is pressure, and η is the viscosity of the gas given by

$$\eta = \frac{M_w \bar{\nu}}{3\sqrt{2}N_o \pi \sigma^2}, \qquad 3.$$

where $\bar{\nu}$ is the mean molecular speed, N_o is the Avagadro constant, and σ is the effective molecular collision diameter. This term K was then adjusted to predict the effective transport coefficient (K_{eff}) of a single gas through a porous body. Using this approach, Wakao et al found that the development of a porous outer layer offers resistance to gas flow giving rise to a moving boundary with a variable concentration of diffusant that depends upon the surface flux,

gas transport coefficient, and thickness of the porous layer. Finally, Tsai (43) coupled intrinsic degradation kinetics with gas flow models to numerically investigate the internal pressure buildup and internal stresses on the particle network of a cylindrical green body during binder thermolysis. The influence of green body size, specific surface area, and pressurized atmosphere was studied.

Strijbos (48) has modeled the removal of carbonaceous residue from porous bodies. Two extreme cases were identified: (*a*) shrinking core model—residue content is high and the body is impenetrable to the gas; in this case, removal is reaction limited and proceeds by an inward movement of a sharp interface between residue-free and residue-filled pores, and (*b*) uniform model—residue content is low and diffusion in this material is not different from gas diffusion in the residue-free material; in this case, removal proceeds uniformly throughout the body when the process is reaction limited. With the exception of this study, little attention has been given to modeling transport processes during the later stages of binder thermolysis.

Transport of volatile species in binder-filled pores occurs by diffusion and has been shown to be rate-limiting during debinding of closed-pore compacts (49, 50). The diffusion rates of various species in solid polymers have been measured in studies of gas transport in membranes, of polymer oxidation, and of gas barrier properties of packaging materials. However, very few data exist on the transport of volatile species or degradation products in polymers at temperatures well above their melting point. As a result, many researchers have simply relied upon order-of-magnitude estimates of diffusion rates when modeling binder removal processes (51–54). Using hot-stage/FTIR microspectroscopy, Lewis & Cima (49) were first to measure the diffusivities of an homologous series of dialkyl phthalate plasticizers in PVB spin-coated thin films, which ranged from 10^{-12} to 10^{-10} cm^2/s for the isotherms investigated (60–150°C). More recently, K Hrdina & J Halloran (unpublished data) have measured the diffusivity of acetic acid, a primary degradation product formed during thermolysis of poly(ethylene-vinyl acetate), in EVA copolymers at elevated temperatures (>100°C). In both cases, diffusion studies were carried out at temperatures below the polymer degradation temperature to avoid complications arising from structural changes in the polymer and the presence of other degradation products. However, additional research is needed in which the diffusion rates of a broad range of species in several common polymeric binders are measured, both above and below their degradation temperatures, to fully optimize binder removal schedules.

Bubble formation is a common occurrence during binder thermolysis of closed-pore compacts. Bubbles form in superheated, molten polymers when temperatures exceed the boiling point of volatile species (e.g. solvents or plasticizers) present within the binder system, or when a local buildup of volatile

degradation products occurs due to mass transfer limitations. Particulate surfaces serve as heterogeneous sites on which bubbles can nucleate. Additional factors that affect the nucleation process at these interfaces include the wetting angle of the fluid on the surface, the curvature of the surface, and the interfacial tension at the liquid-solid surface. Among the variables that affect bubble growth are the surface tension and viscosity of the molten polymer and the diffusivities of the volatile species. These material properties are influenced by thermal variables such as temperature and heating rate (57). Using hot-stage/optical microscopy, Dong & Bowen (56) directly observed bubble nucleation and growth processes in PMMA films that contained residual solvent in both the presence and absence of ceramic particles. Their observations showed that bubbles formed from both residual solvent and polymer degradation products (i.e. MMA monomer) and that bubble nucleation temperatures decreased in the presence of ceramic particles and increased with increasing heating rate.

Calvert & Cima (51) developed a model to predict the kinetics of binder removal from closed-pore compacts containing an unzipping polymer (e.g. PMMA), which decomposes to produce volatile monomeric species. They considered a sheet of ceramic and polymer of thickness $2L$, in which monomer is produced at a rate R_m g/(cm$^3 \cdot$ s) and diffuses at a rate D cm^2/s to the surface. The steady-state concentration of monomer at some distance x from the center line ($x = 0$) is given by

$$C = (R_m/2D)(L^2 - x^2) + C_i, \qquad 4.$$

where C_i is the concentration of monomer in the liquid at the surface. C_i is close to zero if the surrounding gas is rapidly exchanged, and monomer buildup is minimized. They applied their model to PMMA degradation and estimated the rate of MMA formation, the diffusion rates of MMA in the molten binder and gas, and the equilibrium constants between the two phases. In their analysis, gas-phase transport was found to be rapid such that diffusion in the liquid phase was rate controlling. Based on the simple steady-state relation given in Equation 4, the maximum sample thickness that could be successfully debinded at a given temperature without the deleterious formation of bubbles was calculated, as shown in Table 3. The imposed failure criterion was that bubbles would spontaneously form when the concentration of monomer in the green body exceeded that in equilibrium with vapor at 1 atm ($\approx 10^5$ Pa). They concluded that binder removal from parts of more than a few millimeters in thickness would require several days. However, it should be noted that these estimates make no allowance for developing porosity. Calvert & Cima (51) also probed the effects of planar and nonplanar (as would arise from capillary redistribution of molten binder) pore development on the kinetics of binder thermolysis and found that porosity enhances removal rates, particularly in the nonplanar case.

Table 3 Steady-state model maximum thickness for binder thermolysis without defect (bubble) formation

Temperature (°C)	Thickness (mm)	Time to 50% burnout
150	280.00	217 yr
200	20.00	411 d
250	2.5	5.8 d
300	0.42	4.2 h
350	0.088	790 s
400	0.022	64 s

Liquid Redistribution Processes and Scaling Criteria

Capillary forces may act to redistribute thermoplastic binders within the porous network of ceramic green bodies in a manner analogous to drying (49, 50, 58–62). The internal distribution of liquids in porous beds has been the subject of numerous investigations (63–67). Most of the early drying studies centered on the question of whether mass transfer occurred by diffusion or by a different mechanism. Commings & Sherwood (64) and Ceaglske & Hougen (65) clearly showed that liquid motion occurs through the action of local variations in pore suction pressure, which result from variations in particle packing. Liquid-vapor menisci in smaller pores where local particle-packing density is high produce a larger suction potential than do menisci in pores where particle packing is less dense. This relationship is described by the well known Young-Laplace equation:

$$P_s = \frac{2\gamma}{r}, \qquad 5.$$

where P_s is the suction pressure of a pore of radius r, containing a fully wetting liquid-vapor interface with a surface tension γ.

Liquid in an initially saturated porous body evaporates from the surface of the body during drying. The smallest pores at the surface are continually supplied with liquid from the larger pores deep within the body due to the hydrostatic pressure difference created by the difference in their respective suction pressures. Shaw (68) has considered the microscopic distribution of liquids in porous bodies and found that above a critical volume fraction of liquid, a thermodynamic driving force exists to segregate fluid into the smaller pores as removal progresses, as opposed to homogeneously distributing it throughout the body at points (necks) of particle-particle contact. Thus larger pores empty preferentially as drying proceeds.

Three distinct regimes are observed during drying: the constant-rate period (CRP), the first falling-rate period, and the second falling-rate period. In the CRP of drying, mass-transfer control is relegated to the boundary layer between the surface of the body and the free gaseous environment. The observance of the CRP of drying indicates that the external conditions have remained constant during this period, thus permitting the establishment of a boundary layer of constant thickness. The CRP of drying is maintained until liquid can no longer be supplied at a sufficient rate to keep the surface wet, at which point the first falling-rate period of drying is observed. During this period, mass-transfer control is dictated by the rate at which capillarity can supply the surface with fluid. Finally, the second falling-rate period of drying coincides with the onset of the pendular state, in which fluid becomes disconnected and resides solely at the necks (or contacts) between particles. In the pendular state, liquid transport can no longer occur, and the degree of saturation is less than roughly 10%. In this stage, gas-phase transport is the dominate mechanism of drying.

Spronson & Messing (58) were first to suggest that capillary-driven binder redistribution processes occur during debinding of closed-pore compacts on the basis of observations of a constant-rate of binder removal during isothermal TGA studies. In a series of papers, Cima & Lewis (49, 59–61) convincingly demonstrated that capillary-driven liquid-phase transport plays an important role in the thermal debinding of closed-pore, tape-cast ceramic layers, which contain a two-component, thermoplastic binder system. They reported the development of a nonplanar pore front (or binder-vapor interface) as removal progressed (59) and directly observed such processes in two-dimensional binder-filled model pore networks (61). Based on their experimental observations, a model was developed to predict the relative importance of capillary-driven liquid transport based on parameters associated with the binder system, particle bed, and removal conditions (59). Their model equates the driving force for capillary flow as given by (59, 63)

$$\Delta P = \frac{2\Delta\phi\gamma}{d}, \qquad 6.$$

where $\Delta\phi$ accounts for local variations in particle packing, and d is the particle diameter to the viscous pressure drop resulting from flow through a fully saturated porous body as given by

$$\Delta P = \frac{36K\mu}{d^2}\frac{(1-\varepsilon)^2}{\varepsilon^3}hu, \qquad 7.$$

where μ is the viscosity of the fluid, ε is the void fraction of the porous body, and K ($\approx$5) is a constant that accounts for geometrical factors of the pores, such

as their tortuosity and number of constrictions, to yield:

$$\frac{h}{d} = \frac{\Delta\phi\varepsilon^3}{18K(1-\varepsilon)^2}\frac{\gamma}{\nu G}, \qquad 8.$$

where h is the maximum length scale over which capillary forces act, ν ($=\mu/\rho$) is the kinematic viscosity, and G is the mass flux. Close packing of equally sized spheres produces the smallest pores, with $\phi = 12.9$, whereas a simple cubic arrangement of spheres has larger pores, with $\phi = 4.8$. Thus $\Delta\phi = (12.9–4.8) \approx 8$, which represents a conservative estimate of the capillary-driving force because packing in the least-dense areas of the ceramic green body will likely be less dense than cubic packing. The right-hand side of Equation 8 indicates that the characteristic distance h over which capillary-driven liquid migration occurs increases with increasing surface tension. Correspondingly, h decreases as the viscosity and/or mass flux increases because viscous losses become more important, as shown in Figure 7. The critical importance of minimizing binder viscosity (and, hence, flow resistance) was also noted in modeling work on binder thermolysis carried out by Stangle & Aksay (62).

The advantages of capillary-driven liquid transport on binder removal kinetics were first demonstrated by Lewis & Cima (49). In their work, dibutyl phthalate (DBP) plasticizing species were preferentially removed from highly-loaded, tape-cast ceramic layers in isothermal TGA studies. A CRP of plasticizer removal was observed at temperatures below the onset of degradation of the polymeric constituent PVB. The observance of a CRP of removal during debinding of a two-component, graded-volatility binder system requires that the controlling mass transport distance remains constant as removal proceeds, not that removal occurs at the component surface. In this situation, the characteristic diffusion length (l) was shown to correspond to the distance between emptying pores connected to the exterior surface of the porous body. The calculations were made by relating the mass flux (J) of DBP removed from the tapes during I-TGA to the effective plasticizer diffusivity (D_{eff}) within the binder-filled pore network as given by (49)

$$J = -D_{\text{eff}}\frac{\Delta c}{l}, \qquad 9.$$

where Δc is the concentration gradient and D_{eff} is given by

$$D_{\text{eff}} = \frac{D\varepsilon}{\tau}, \qquad 10.$$

where D is the diffusivity of DBP, ε is the void fraction, and τ ($\approx$5) is the tortuousity factor. Enhanced plasticizer removal rates were largely attributed to the reduction in the characteristic diffusion length (l) resulting from capillary-driven liquid transport. In this case, the diffusion distance no longer depends on

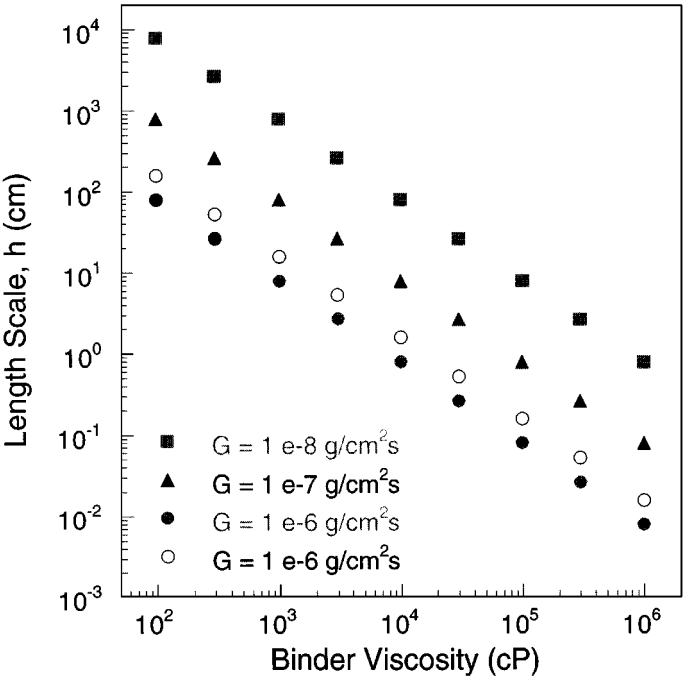

Figure 7 Plot of characteristic length scale h over which capillary-driven liquid transport occurs as a function of binder viscosity for varying volatile removal rates. (Calculations were carried out using Equation 8, assuming $\Delta\phi = 8$, $\varepsilon = 0.4$, $\gamma = 10^{-5}$ N/cm (10 dyne/cm), and $K = 5$. Solid symbols denote values calculated for $d = 0.5$ μm, and open symbols denote values calculated for $d = 1$ μm.)

the component dimensions, but rather on the distance between large penetrating pores (which is on the order of several particle diameters) (49). Additional evidence for the importance of these mass transport processes was recently reported by Angermann and coworkers (53, 54) who studied thermal debinding of injection-molded components containing a two-component, graded-volatility binder system. Invoking the above analysis, they estimated characteristic diffusion lengths of several particle diameters, suggesting that capillary-driven binder redistribution also occurred for their system.

Recently, Lewis et al (69) carried out a series of computer simulations to further investigate the removal of multicomponent, thermoplastic binders from two- and three-dimensional model particulate bodies. Simulations were carried out under isothermal conditions to study the influence of liquid-phase transport processes, i.e. volatile diffusion in binder-filled pores and capillary driven

redistribution of the binder phase, on plasticizer removal rates. Plasticizer removal was modeled by a random-walk algorithm (70–75), and nonplanar pore development arising from capillary migration of binder was modeled by an invasion percolation algorithm (76, 77). For comparison, simulations were also carried out on systems in which binder redistribution was not permitted. In such cases, pore development was modeled as an advancing or nonadvancing planar front. Visualization of transport phenomena at the microscopic level has provided the first quantitative assessment of plasticizer concentration profiles as a function of time $C(t)$ and depth $C(z)$ and binder-vapor interfacial development during removal. Removal rates were significantly enhanced when capillary-driven binder redistribution was assumed, as shown in Figure 8 for a highly loaded three-dimensional system with an initial binder composition

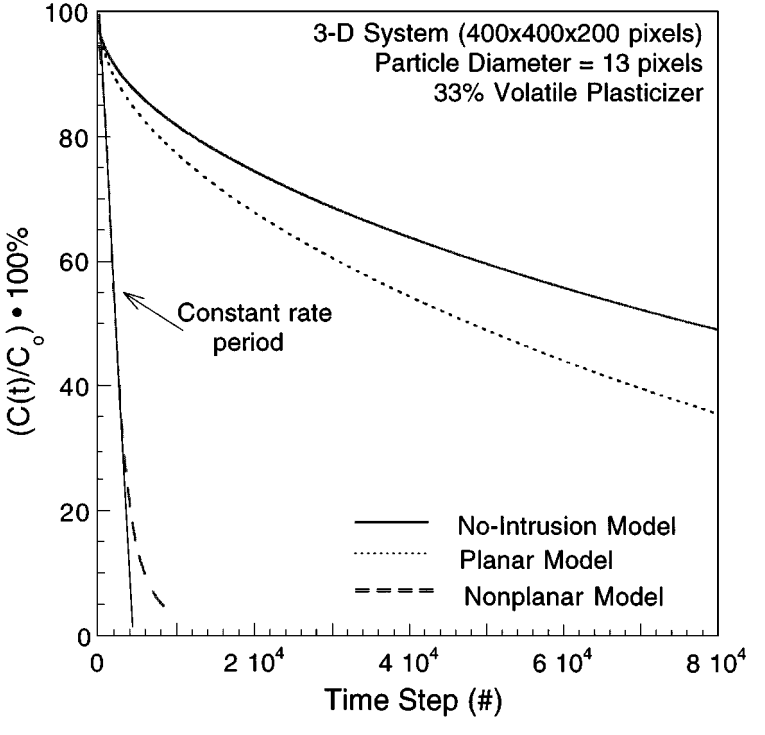

Figure 8 Plot of plasticizer loss (% of initial content) as a function of time for the three-dimensional model system ($400 \times 400 \times 200$ pixels) containing approximately 57% monosized spheres (diameter $=$ 13 pixels) and 43% binder with an initial composition of 33% volatile (plasticizing) species for the no-intrusion, planar, and nonplanar models.

of 33% plasticizing and 67% nonvolatile, polymeric species. It is noteworthy that a constant rate of plasticizer removal was observed for the nonplanar (capillary-driven) model analogous to the experimentally observed behavior outlined above for tape-cast ceramic layers with identical binder loading and composition.

PROCESS DESIGN

The intelligent design of optimal binder removal processes hinges critically on understanding the influence of several parameters, including those associated with the binder system (e.g. loading, composition, polymer degradation chemistry, viscosity, surface tension, and volatile properties such as diffusivities, vapor pressure, boiling point, etc), the component (e.g. particle size, packing density and uniformity, surface chemistry and interactions), and the thermolysis process (e.g. temperature-time-atmosphere control). Successful debinding of ceramic green bodies clearly requires a delicate balance between the generation rate of volatile constituents and their removal rates and the minimization of sharp concentration (hence, stress) gradients within the porous body to avoid the formation of defects.

Important criteria for binder design can be derived from the discussions of polymer degradation and mass transport processes provided in this review. Ideally, binder loadings should be minimized when possible to provide an open, continuous network of empty pores in the as-formed green body. If forming method requirements prohibit this, then multicomponent binder systems should be utilized containing appreciable amounts of volatile species (e.g. plasticizers) that can be preferentially eliminated in a two-stage debinding sequence such that sufficient empty pore space is generated prior to polymer degradation events. It should be noted that polymer degradation is difficult to control, and additives that degrade gradually over a broad temperature range are most suitable, as opposed to unzipping polymers. However, careful consideration must be given to the deleterious impact of increased carbon residue formation, which is likely to occur in the former case. Finally, the physical properties of the binder system should also be tailored to minimize mass-transfer resistance, including the binder viscosity and volatile diffusivities (generally size dependent).

Important criteria for green body design can also be derived from the above discussions of polymer degradation and mass transport processes during thermolysis. Clearly, the selection of compatible ceramic-organic chemistries to avoid undesirable catalysis of degradation events or extrinsic formation of involatile carbon residues is optimal. In addition, mass-transfer resistance has been shown to be minimized with increasing particle size and void fraction. Such parameters significantly influence the final properties of the sintered

components and, thus, cannot often be tailored solely for the purpose of improving binder removal.

The optimization of binder removal schedules (i.e. temperature-time-atmosphere) can be readily achieved provided a thorough understanding of the complex physico-chemical events that occur during debinding of a given ceramic green body exists. Current deficiencies in this knowledge base, however, have led to the development of various process control algorithms predicated on trial-and-error design experiments, which focus mainly on first identifying the maximum weight loss rate (dW/dt) that can be achieved during debinding without the introduction of deleterious defects, and then designing removal schedules in which this maximum weight loss rate is not exceeded (78–81). Although this represents some improvement over earlier approaches, it remains rather simplistic and does not account for the fact that acceptable maximum weight loss rates are likely to vary significantly as thermolysis proceeds.

CONCLUDING REMARKS

Binder removal has been shown to be a critical processing step in the manufacture of ceramic components. Some of the physico-chemical processes that occur during binder removal from ceramic green bodies have been reviewed in this paper. Representative examples of intrinsic degradation mechanisms for common polymeric additives were discussed. However, even for the simplest of cases, such mechanisms were shown to become highly complicated in the presence of ceramic surfaces. These complications present experimental difficulties that limit our knowledge of the reaction kinetics, the composition of degradation products, and the nature of various side reactions that lead to the formation of involatile carbonaceous residue, particularly in the presence of ceramic surfaces with complex chemistries. Various mass transfer mechanisms were also discussed with emphasis on gas-phase transport in empty pores, and on liquid-phase transport processes such as volatile transport in binder-filled pores and capillary-driven binder redistribution. The limited experimental work carried out to quantify mass transfer parameters such as volatile diffusivities in polymeric additives was reviewed. Again, experimental difficulties arise due to complications stemming from degradation-induced structural changes in the polymer matrix and/or formation of additional diffusing species, which have relegated previous studies to temperatures below the onset of degradation. A review of simplistic models developed to account for such events was also presented. In most cases, these models have been applied to treat only simple situations, such as debinding of an unzipping polymer in which only monomeric degradation products are considered or selective removal of volatile species under isothermal conditions at temperatures below the onset of

polymer degradation. Although models with the level of sophistication necessary to simultaneously account for multiple degradation reactions, heat/mass transfer considerations, and interrelated dependencies have yet to be implemented, some basic design criteria for optimizing binder systems and removal sequences were elucidated from present efforts and briefly discussed.

ACKNOWLEDGMENTS

I would like to thank M Cima, W Rhine, R Higgins, and HK Bowen for many fruitful discussions of issues related to binder removal from ceramics. In addition, I would like to express my gratitude to A Read and S Morissette for their invaluable assistance in the preparation of this manuscript.

Literature Cited

1. Whittemore JW. 1944. *Bull. Am. Ceram. Soc.* 23:427–32
2. Wild A. 1954. *Ceram. Bull.* 33:368–70
3. Cowan RE, Ehart EP. 1966. *Ceram. Bull.* 45:535–38
4. Andrews PW, Peters FI. 1969. *U.S. Patent No. 3,472,803*
5. Pincus AG, Shipley IE. 1969. *Ceram. Ind.* 92:106–9; 146
6. Levine SL. 1969. *Ceram. Bull.* 48:230–31
7. Hoffman ER. 1972. *Ceram. Bull.* 51:240–42
8. Salamone AL, Reed JS. 1979. *Ceram. Bull.* 58:618–19
9. Harvey JW, Johnson DL. 1980. *Ceram. Bull.* 59:637–39
10. Mizuno KM, Takata M, Yanagida H. 1978. *Ceram. Bull.* 57:519–21
11. McNamara EP, Comefora JE. 1945. *J. Am. Ceram. Soc.* 28:25–31
12. Onoda GY. 1978. The rheology of organic binder solutions. In *Ceramic Processing Before Firing*, ed. GY Onoda, LL Hench. pp. 235–51. New York: Wiley and Sons
13. Platzer NAJ. 1965. Plasticization and plasticizer processes. In *Advances in Chemistry*, ed. NAJ Platzer, Ser. 48. Washington, DC: Am. Chem. Soc.
14. Fujita H, Kishimoto A. 1958. *J. Polym. Sci.* 28:547–67
15. Boyer RF, Spencer RS. 1947. *J. Polym. Sci.* 2:157–77
16. Higgins RJ. 1990. *The chemistry of carbon retention during non-oxidative binder removal from ceramic greenware*. PhD thesis. Massachusetts Institute of Technology, Cambridge. 165 pp.
17. Jellinek HHG. 1978. Degradation and depolymerization kinetics. In *Aspects of Degradation and Stabilization of Polymers*, ed. HHG Jellinek, pp. 1–37. Amsterdam/Lausanne/New York: Elsevier
18. Grassie N, Melville HW. 1949. *Proc. R. Soc. London Ser. A* 199:24–39
19. Madorsky SL. 1956. *J. Polym. Sci.* 11:491–506
20. MacCallum JR. 1965. *Makromol. Chem.* 83:137–47
21. Cameron GG, Kerr GP. 1968. *Makromol. Chem.* 115:268–74
22. Kashiwagi T, Hirata T, Brown JE. 1985. *Macromolecules* 18:131–38
23. Gritter RJ, Seegor M, Johnson DE. 1978. *J. Polym. Sci. Polym. Chem. Ed.* 16:169–77
24. Sun Y-N, Sacks MD, Williams JW. 1988. In *Ceramic Powder Science IIA*. ed. GL Messing, E Fuller, H Hausner. pp. 538–48. Westerville, OH: Am. Ceram. Soc.
25. Madorsky S, Strauss S. 1959. *J. Polym. Sci.* 36:183–94
26. Bakht MF. 1983. *Pak. J. Sci. Ind. Res.* 26:35–40
27. Cima MJ, Lewis JA. 1988. In *Ceramic Powder Science IIA*. ed. GL Messing, E Fuller, H Hausner. pp. 567–74. Westerville, OH: Am. Ceram. Soc.
28. Shih W-K, Sacks MD, Schieffle GW, Sun Y-N, Williams W. 1988. In *Ceramic Powder Science IIA*. ed. GL Messing, E Fuller,

H Hausner. pp. 549–58. Westerville, OH: Am. Ceram. Soc.
29. Howard KE, Lakeman CDE, Payne DA. 1990. *J. Am. Ceram. Soc.* 73:2543–46
30. Hall JW, Rase HF. 1963. *Ind. Eng. Chem. Proc. Des. Dev.* 2:25–30
31. Eberly PE, Kimmerlin CN, Miller WH, Drushel HV. 1966. *Ind. Eng. Chem. Proc. Des. Dev.* 5:193–98
32. Eisenbach D, Gallei E. 1979. *J. Catalysis* 56:377–89
33. Langner BE. 1981. *Ind. Eng. Chem. Proc. Des. Dev.* 20:326–31
34. Billmeyer F. 1984. *Textbook of Polymer Science*, New York: Wiley and Sons. 3rd ed.
35. Gates BC, Katzer JR, Schuit CGA. 1978. *Chemistry of Catalytic Processes.* New York: McGraw-Hill
36. Higgins RJ, Rhine WE, Cima MJ, Bowen HK. 1994. *J. Am. Ceram. Soc.* 77:2243–53
37. Ai J, Phegley LL, Christen G, White RL. 1995. *J. Am. Ceram. Soc.* 78:874–80
38. Hirakata K, Rhine WE, Cima MJ. 1996. *J. Am. Ceram. Soc.* 79:1002–8
39. Kemp D, Vellachio F. 1980. *Organic Chemistry.* New York: Worth
40. Yan H, Cannon WR, Shanefield DJ. 1993. *J. Am. Ceram. Soc.* 76:166–72
41. Nair A, White R. 1996. *J. Appl. Polym. Sci.* 60:1901–9
42. German RM. 1979. *Intl. J. Powder Metall. Powder Tech.* 15:23–30
43. Tsai D-S. 1991. *AIChE J.* 37:547–54
44. Song JH, Edirisinghe MJ, Evans JRG, Twizell EH. 1996. *J. Mater. Res.* 11:830–40
45. Knudsen M. 1909. *Ann. Phys.* 28:75
46. German RM. 1987. *Intl. J. Powder Metall.* 23:237–45
47. Wakao N, Otani S, Smith JM. 1965. *AIChE J.* 11:435
48. Strijbos S. 1973. *Chem. Eng. Sci.* 28:205–13
49. Lewis JA, Cima MJ. 1990. *J. Am. Ceram. Soc.* 73:2702–7
50. Barone MR, Ulciny JC. 1990. *J. Am. Ceram. Soc.* 73:3323–33
51. Calvert P, Cima MJ. 1990. *J. Am. Ceram. Soc.* 73:575–79
52. Matar SA, Edirisinghe MJ, Evans JRG, Twizzell EH. 1996. *J. Am. Ceram. Soc.* 79:749–55
53. Angermann HH, Yang FK, Van der Biest OO. 1992. *J. Mater. Sci.* 27:2534–38
54. Angermann HH, Van der Biest OO. 1993. *Intl. J. Powder Metall.* 29:239–50
55. Deleted in proof
56. Dong C, Bowen HK. 1989. *J. Am. Ceram. Soc.* 72:1082–87
57. Street JR, Fricke AL, Reiss LP. 1971. *Ind. Eng. Chem. Fundam.* 10:54–64
58. Spronson DW, Messing GL. 1988. In *Ceramic Powder Science IIA.* ed. GL Messing, E Fuller, H Hausner. pp. 549–58. Westerville, OH: Am. Ceram. Soc.
59. Cima MJ, Lewis JA, Devoe AD. 1989. *J. Am. Ceram. Soc.* 72:1192–99
60. Cima MJ, Dudziak M, Lewis JA. 1989. *J. Am. Ceram. Soc.* 72:1087–90
61. Lewis JA, Cima MJ. 1990. In *Ceramic Transactions*, ed. GL Messing, H Hausner, S Hirano, 12:583–90. Westerville, OH: Am. Ceram. Soc.
62. Stangle GC, Aksay IA. 1990. *Chem. Eng. Sci.* 45:1719–31
63. Haines WB. 1927. *J. Agri. Sci.* 17:264
64. Commings EW, Sherwood TK. 1934. *Ind. Eng. Chem.* 26:1096–98
65. Ceaglske NH, Hougen OA. 1937. *Trans. Am. Inst. Chem. Eng.* 33:283–314
66. Pearse JF, Oliver TR, Newitt DM. 1949. *Trans. Inst. Chem. Eng.* 27:1
67. Scott VH, Corey AT. 1961. *Soil Sci. Soc. Proc.* 270–74
68. Shaw TM. 1986. *J. Am. Ceram. Soc.* 69:27–34
69. Lewis JA, Galler MA, Bentz DP. *J. Am. Ceram. Soc.* 79:1377–88
70. King GW. 1951. *Ind. Eng. Chem.* 43:2475–77
71. Murch GE, Thorn RJ. 1979. *Philos. Mag. A* 39:673–77
72. Majerus MS, Soong DS, Prausnitz JM. 1984. *J. Appl. Polym. Sci.* 29:2453–66
73. Brandt WW. 1973. *J. Chem. Phys.* 59:5562–70
74. Kim IC, Torquato S. 1990. *J. Appl. Phys.* 68:3892–903
75. Bentz DP, Nguyen T. 1990. *J. Coat. Technol.* 62:57–63
76. Wilkinson D, Willemsen JF. 1983. *J. Phys. A: Math. Gen.* 16:3365–76
77. Willemsen JF. 1986. *Prog. Theor. Phys. Suppl.* 86:399–405
78. Sakai T, Inoue M, Kihara Y, Kawabata Y. 1985. *Jpn. Patent No. 215577*
79. Johnsson A, Carlstrom E, Hermansson L, Carlsson R. 1983. *Proc. Br. Ceram. Soc.* 33:139–47
80. Johnsson A, Carlstrom E, Hermansson L, Carlsson R. 1983. *Mater. Sci. Monogr.* 16:767–72
81. Verweij H, Bruggnik WHM. 1990. *J. Am. Ceram. Soc.* 73:226–31

Annual Review of Materials Science
Volume 27, 1997

CONTENTS